STRUCTURAL
BIOLOGY

Volume 74 (2018)

Supporting information for article:

The crystal structure of the malic enzyme from *Candidatus* Phytoplasma reveals the minimal structural determinants for a malic enzyme

C. E. Alvarez, F. Trajtenberg, N. Larrieux, M. Saigo, A. Golic, C. S. Andreo, S. A. Hogenhout, M. A. Mussi, M. F. Drincovich and A. Buschiazzo

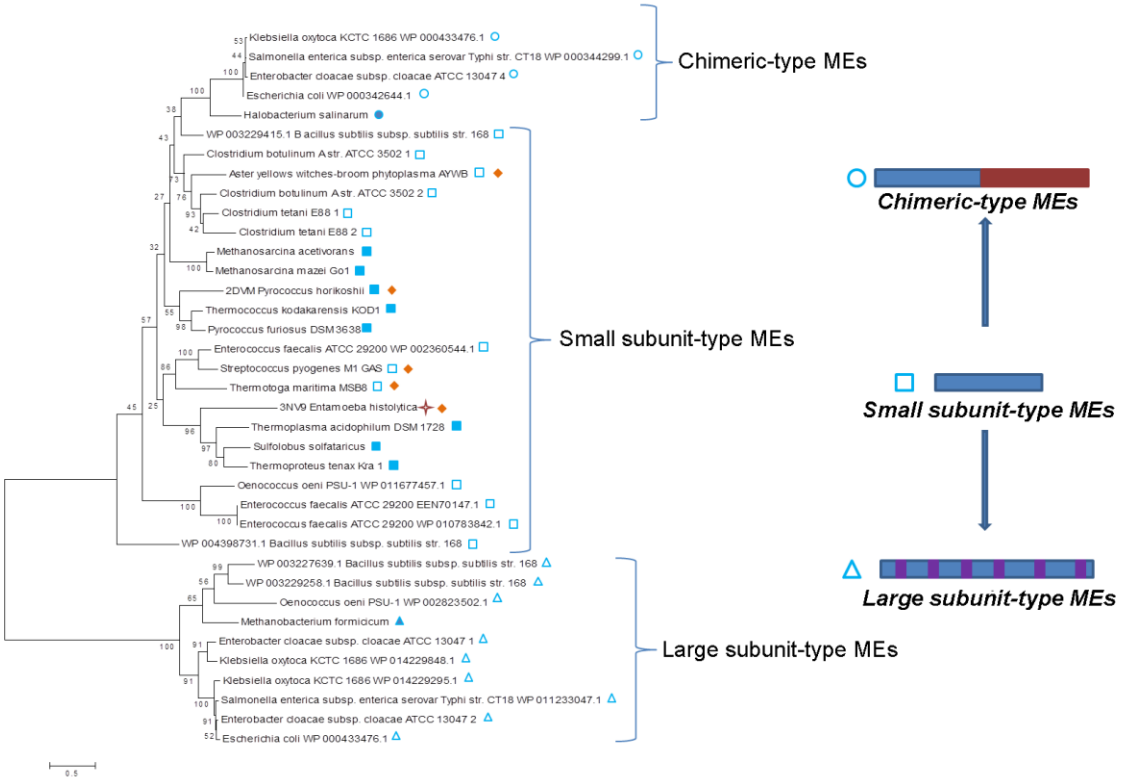

Figure S1 Phylogenetic relationships among members of the ME family found in different taxa such as archaea, bacteria and a unicellular eukaryote (*Entamoeba histolytica*). Open symbols indicate eubacterial sources of protein sequences, whereas closed symbols indicate archaeal ones. MEs with known crystal structures are indicated with orange diamonds. On the right side, two possible routes of evolution are shown, starting from small subunit-type MEs (open squares) to large subunit-type MEs (open triangles) and chimeric MEs (open circles). The red star indicates the ME from the eukaryote *E. histolytica* (AAF43042.1). The tree was constructed analyzing 37 amino acid sequences and drawn to scale, with branch lengths measured in number of substitutions per site. All positions with less than 80% site coverage were eliminated. That is, fewer than 20% alignment gaps, missing data, and ambiguous bases were allowed at any one position. A total of 386 positions were thus included in the final dataset. Evolutionary analyses were conducted with MEGA7 (Kumar *et al.*, 2016). Sequences retrieved from the genomes of the following organisms were used: *Enterobacter cloacae*; *Klebsiella oxytoca*; *Salmonella enterica*; *Escherichia coli*; *Halobacterium salinarum*; *Bacillus subtilis*; *Clostridium botulium*; *Ca.* Phytoplasma *AYWB*; *Clostridium tetani*; *Methanosarcina acetivorans*; *Methanosarcina mazei*; *Enterococcus faecalis*; *Oenococcus oeni*; *Streptococcus pyogenes*; *Thermotoga maritima*; *Thermoplasma acidophilum*; *Sulfolobus solfataricus*; *Thermoproteus tenax*;

Entamoeba histolytica; *Thermococcus kodakarensis*; *Pyrococcus furiosus*; *Methanobacterium formicicum.*

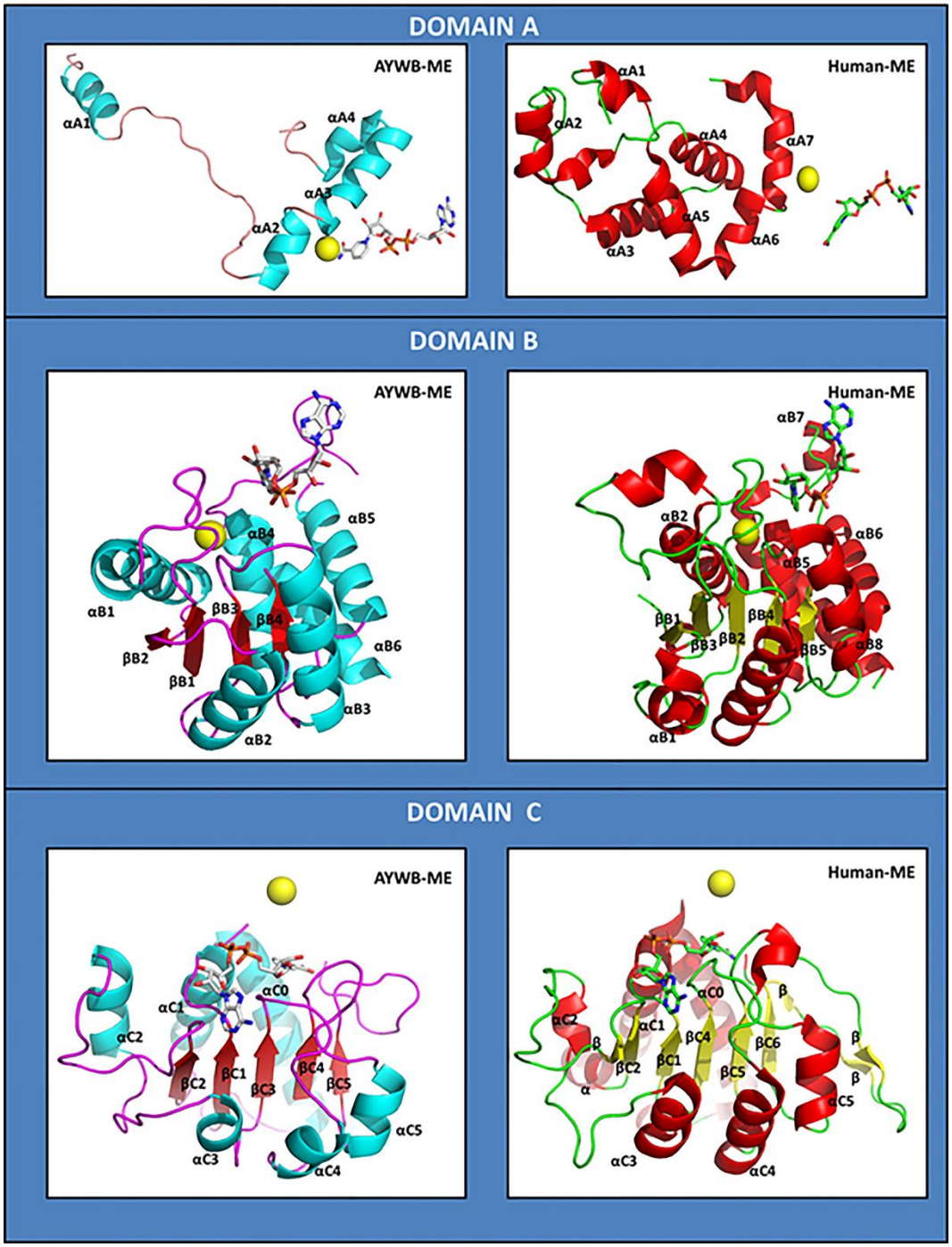

Figure S2 Comparison of the structure of domains A, B and C of AYWB-ME and Human-ME. The conformation of each domain from AYWB-ME (left) and Human-ME (right) are shown. The number of each secondary structure element (Figure 1A) is indicated. NAD is shown as a stick model and Mg^{2+} as a yellow sphere.

NAD moiety	Atoms of NAD/ residue protein		Distance (A)	
	Human-ME	AYWB-ME	Human-ME	AYWB-ME
Adenine ribose	AO2'/ K346 NH	AO2'/N285O	3.1	
	AO3'/A312NH	AO3'/N285NH	3.2	3.5
	AO3'/G313NH		3.4	
		AN2/K216Nω		3.5
Biphosphate	NO1'/ R165 Nω	NO1/S194NH	3.0	3.2
	AO1/ N259NH		2.7	
	NO2/ E314 NH		3.3	
	NO/A315O		2.9	
		AO2/A195		3.2
Nicotinamide ribose	NO3'/N421NH		3.4	
	NO2'/N421NH	NO2'/D215 O	2.8	2.4
		NO2'/D215 O	2.8	2.8
	NO2'/N421Nδ			
Nicotinamide	NO7/ G446C		3.1	
	NN7/G465O	NN7/N316O	2.6	2.7
		NN7/V314O		3.2
	NN7/N467Oδ		3.1	

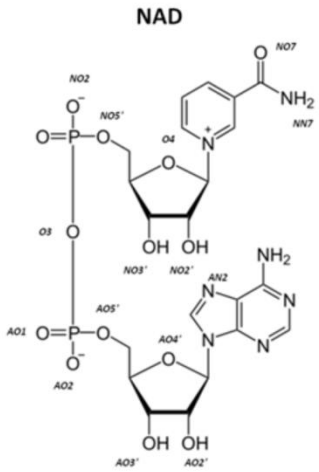

Figure S3 Residues involved in NAD binding comparing AYWB-ME with Human-ME. A comparison of binding distances involved in the interaction of the NAD cofactor is shown for Human-ME

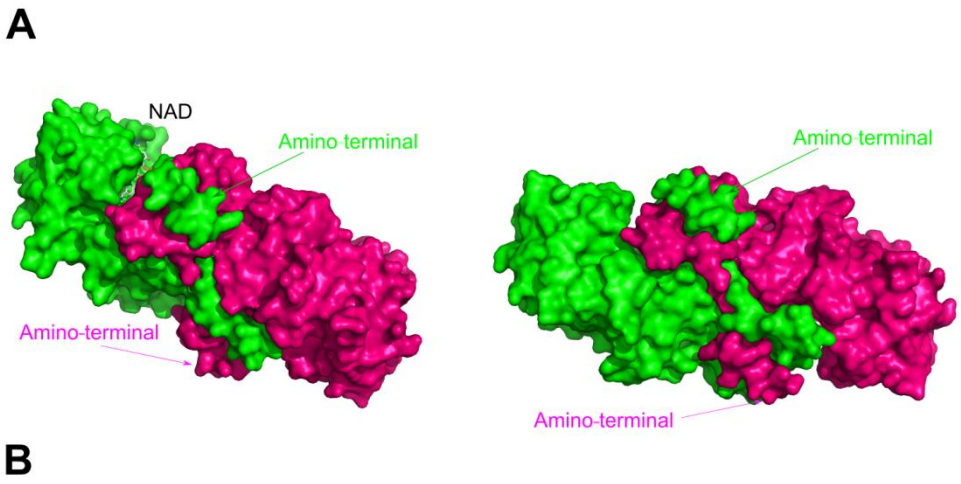

	AY-WB ME (5CEE)	Human-ME (1DO8)
Total oligomer surface (Å²)	28.350 (dimer)	76.520 (tetramer)
Buried oligomer surface (Å²)	10.810 (5.405/monomer)	25.650 (6.413/monomer)
N residues at the dimer interface	105	58
Dimer interface surface (Å²)	4.189 (-80.3 kcal/mol)	2.177 (-18.2 kcal/mol)

Figure S4 Analysis of the dimer interface. **A)** Surface representation of AYWB-ME showing the tight interaction between the two protomers, which are shown in pink and green. **B)** Comparison of PISA interface figures between AYWB-ME and Human-ME. The total oligomeric surface areas; the

solvent-buried surface areas; the number of dimer interfacing residues; and the dimer interface area, are compared.

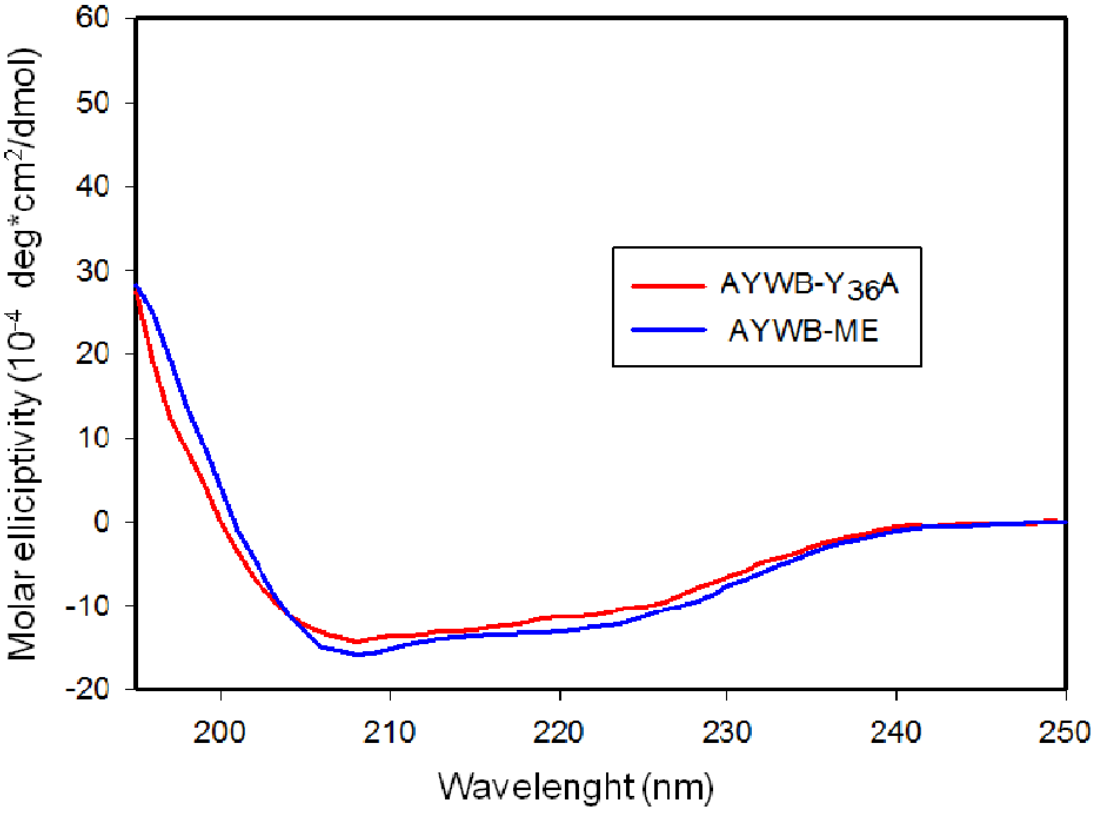

Figure S5 Secondary structure comparative analysis of the wild-type AYWB-ME and the AYWB-Tyr_{36}Ala mutant. CD spectra of AYWB-ME (blue line) and AYWB-Tyr36Ala (red line), do not show significant differences.